Evaluation of Parametric Significance in Friction Welding Process for AA2024-T6 and Zr705 Alloy using Finite Element Analysis

Chennakesava R Alavala
JNTUH College of Engineering, Kukatpally,
Hyderabad, Telangana State, Pin:500085, India

Abstract— **The objective of this work was to evaluate the process parameters of friction welding of AA2024 and Zr705 alloy. Finite element analysis was adopted to analyze the friction welding process. The process parameters were frictional time, frictional pressure, rotational speed and forging pressure. The joints were evaluated for their strength, bulk deformation, penetration and flange formation. The heat affected zone and metal flow across the weld joints were also studied. For friction welding of AA2024-T6 and Zr705 alloy, the major process parameters were forging pressure, friction time and rotation speed.**

Keywords— *AA2024-T6, Zr705alloy, frictional time, frictional pressure, rotational speed and forging pressure, friction welding.*

I. INTRODUCTION

In the friction welding process, friction heats the material to a plastic state in conjunction with an applied force to create the weld [1, 2, 3]. Friction welding of dissimilar metals accounts for nearly half of the welds made by the process [4, 5, 6].

Aluminum alloy 2024 is an aluminum alloy, with copper as the primary alloying element. Typical applications of AA2024 alloy are aircraft fittings, gears and shafts, bolts, clock parts, computer parts, couplings, fuse parts, hydraulic valve bodies, missile parts, munitions, nuts, pistons, rectifier parts, worm gears, fastening devices, veterinary and orthopedic equipment, structures. Zirconium 705 alloy is alloyed with Niobium to increase its strength and improve its formability. Zirconium cannot be fusion-welded to most other common construction metals such as copper, nickel, or iron. Zirconium forms brittle intermetallic compounds with these alloys - compounds that result in cracking. The quality of a weld is most often judged by the strength of the weld and the strength of the material around it. To conventionally friction weld a Zircaloy workpiece 20 to a stainless steel workpiece 19, if the workpieces are from 2.54 mm to 6.35 mm in diameter, the workpieces should be rotated relative to each other at a speed of over 600 rpm while forcing the workpieces together with a force of between 138 and 414 MPa for less than three seconds [7].

The objectives of present work were to investigate the influence of process parameters on weld strength, bulk deformation and metal flow during the conventional friction welding of the AA2024-T6 and Zr705 alloy. Concentration was focused on different circumstances of rotational speed, frictional pressure, frictional time and forging pressure. The experiments were planned using Taguchi techniques; the frictional welding was modeled using finite element analysis (FEA).

II. FINITE ELEMENT MODELING

In this study, ANSYS WORKBENCH (15.0) software was used in the coupled deformation and heat flow analysis during friction welding of the AA2024-T6 and Zr705 alloy. An axisymmetric 3D model of the AA2024-T6 and Zr705 alloy s of 25.4 mm diameter and 100 mm length were made using ANSYS workbench as shown in Fig. 1. Tetrahedron elements were used to mesh the AA2024-T6 and Zr705 alloy rods. The rotating part (AA2024-T6) and the non-rotating part (Zr705alloy) were meshed with 3298 elements / 14904 nodes and 3672 elements / 16493 nodes correspondingly.
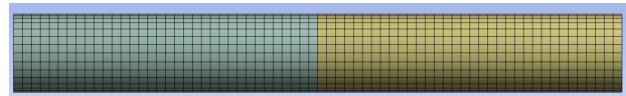

Fig.1. Finite element modeling of friction welding

First the transient thermal analysis was carried out staying the Zr705 alloy rod stationary and the AA2024-T6 rod in rotation. The coefficient of friction 0.2 was applied at the interface of the AA2024-T6 and Zr705 alloy rods. The convection heat transfer coefficient was applied on the surface of two rods. The heat flux calculations were imported from ANSYS APDL commands and applied at the interface. The temperature distribution was evaluated. The thermal analysis was coupled to the static structural analysis [8]. For the structural analysis the rotating (AA2024-T6) rod was brought to stationary and the forging pressure was applied on the Zr705 alloy rod along the longitudinal axis. The Zr705 alloy rod was allowed to move in the axial direction [9]. The structural analysis was carried out for the equivalent stress, bulk deformation and penetration.

The modeling and analysis of the friction welding was carried out as per the design of experiments using Taguchi techniques. The process parameters and their levels are given

table-1. The orthogonal array (OA), L9 was selected for the present work. The assignment of parameters along with the OA matrix is given in Table 2.

TABLE I.   PROCESS PARAMETERS AND LEVELS

Factor	Symbol	Level–1	Level–2	Level–3
Frictional Pressure, MPa	A	25	30	35
Frictional time, Sec	B	3	4	5
Rotational speed	C	1500	2000	2500
Forging pressure, MPa	D	1.25A	1.50A	1.75

TABLE II.   ORTHOGONAL ARRAY (L9) AND CONTROL PARAMETERS

Trial No.	A	B	C	D
1	1	1	1	1
2	1	2	2	2
3	1	3	3	3
4	2	1	2	3
5	2	2	3	1
6	2	3	1	2
7	3	1	3	2
8	3	2	1	3
9	3	3	2	1

III.   RESULTS AND DISCUSSION

The results obtained from the finite element analysis were verified experimentally on the selective trials. The statistical Fisher's test was carried out to find the acceptable all process parameters at 90% confidence level.

A.   Influence of parameters on temperature distribution

Table – 3 gives the ANOVA (analysis of variation) summary of temperature distribution. Even though all the process parameters could satisfy the Fisher's test at 90% confidence level, only frictional pressure and rotational speed made major contribution in the total variation of temperature. The frictional pressure (A) and rotational speed (C) conferred, respectively, 55.15% and 38.53% of the total variation in the temperature. The contribution of frictional time (B) was negligible. Forging pressure (D) had a little influence of 6.25%.

TABLE III.   ANOVA SUMMARY OF THE TEMPERATURE DISTRIBUTION

Source	Sum 1	Sum 2	Sum 3	SS	v	V	F	P
A	5785.66	6622.14	7753.1	324977.2	2	162488.6	462	19.81
B	5278.23	7106.13	7776.54	557345.6	2	278672.8	792	34.01
C	5236.87	6753.63	8170.4	717410.9	2	358705.5	1020	43.79
D	7080.43	6987755	20160.9	33838.89	2	16919.5	48	2.02
e	23381.19	7008237	43860.94	3164.99	9	351.666	1.00	0.37
T	5785.66	6622.14	7753.1	1636737.6	17			100

Note: SS is the sum of square, v is the degrees of freedom, V is the variance, F is the Fisher's ratio, P is the percentage of contribution and T is the sum squares due to total variation.

The temperature developed in the welding rods was directly proportional to the frictional pressure, frictional time and rotational speed as shown in Fig. 2, 3 and 4, respectively. In

fact this is natural phenomena. The conditions of trial 9 gave the highest temperature (1535.6^{o}C) generation and trial 1 gave the lowest temperature (538.43^{o}C) generation in the rods. For trial 9, the frictional pressure and time were, respectively 50 MPa and 5 sec; whereas these were 30 MPa and 3 sec respectively for the trial 1 (Fig. 4).
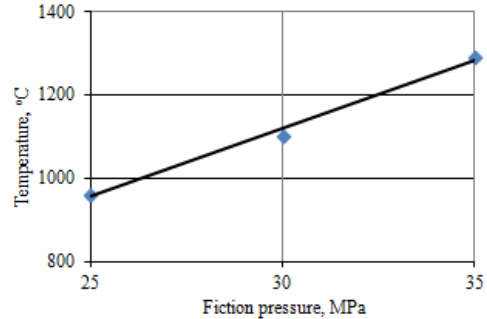
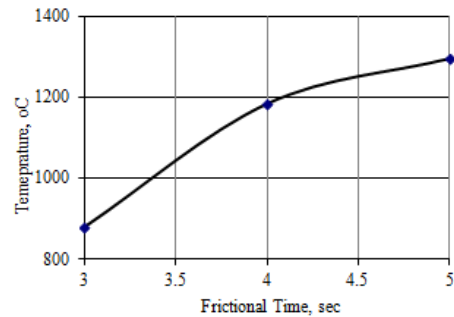Fig. 2. Influence of frictional pressure on temperature.

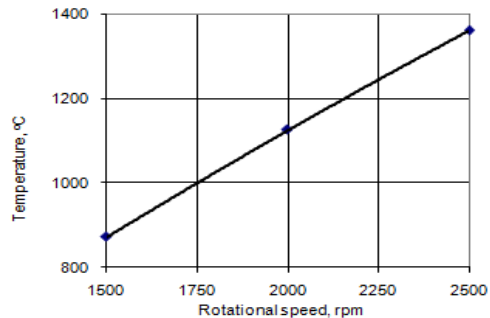Fig. 3. Influence of frictional time on temperature.

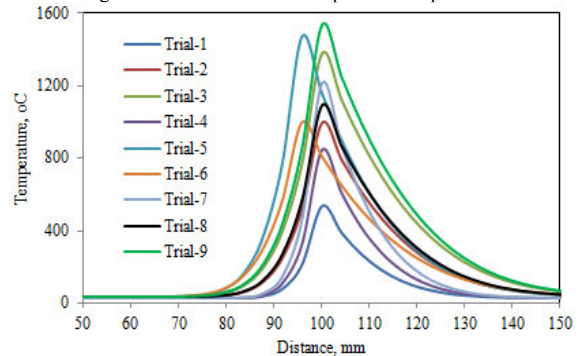Fig. 4. Influence of rotational speed on temperature.

Fig. 4. Temperature distribution during different trials.

B.   Influence of parameters on equivalent stress

The ANOVA summary of the equivalent stress is given in Table 4. The process parameters which were acceptable

through Fisher's test at 90% confidence level were frictional pressure (A), friction time (B), rotational speed (D) and forging pressure as the Fisher's ratio was greater than 3.01. The contributions of frictional pressure (A) and rotational speed (D) were, respectively, 34.36%, and 62.52% towards the total variation of effective stress.

TABLE IV.   ANOVA SUMMARY OF THE EQUIVALENT STRESS

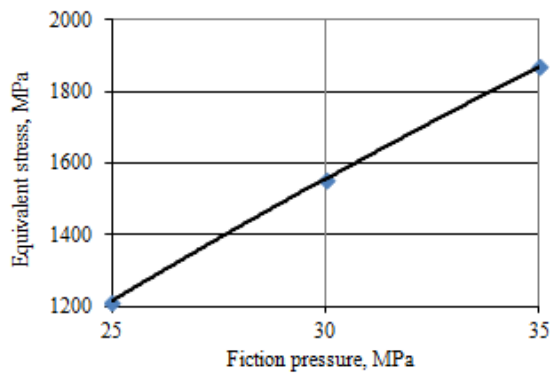| Source	Sum 1	Sum 2	Sum 3	SS	v	V	F	P
A	7289.39	9336.6	11217.5	1286605.7	2	643302.83	5594.30	34.36
B	9731.29	8638.1	9474.1	108894.83	2	54447.415	473.49	2.9
C	6559.19	9479	11805.3	2303257.4	2	1151628.7	10014.82	61.52
D	8926.79	15527816	27843.5	43933.98	2	21966.99	191.03	1.17
e				1034.9321	9	114.99246	1.00	0.05
T	32506.66	15555270	60340.4	3743726.8	17			100

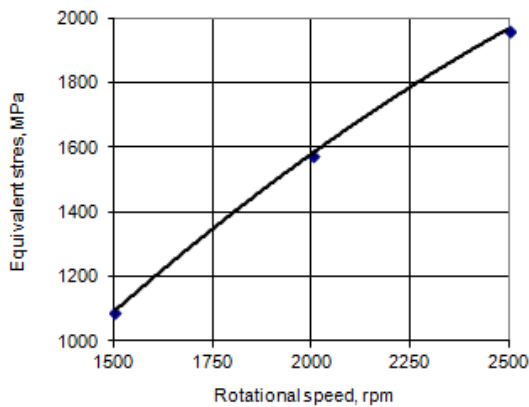Fig. 5 Influence of frictional pressure on equivalent stress.

Fig. 6 Influence of rotational speed on equivalent stress.

The equivalent stress increased with increase of the frictional pressure and rotational speed as shown in Fig. 5 and 6. The stresses induced in the HAZ were of thermal stresses due to frictional heat and of structural stresses owing to applied frictional pressure, frictional time and rotating speed (Fig. 7). This is because the frictional heat is a function of pressure applied on the rods, contact time of the rods and the rotating speed of the rotational member. During joining of aluminum and copper materials using friction welding,. tensile strength of the joints increased up to a peak strength then decreased [10]. The severe plastic deformation which occurs

along the weld interface has an effect on the fracture of grains. As the metal turns and flows in the plane of the weld interface, intermetallic compounds are swept along and subjected to high temperatures and triaxial stresses. As a result of this thermomechanical processing, the intermetallic compounds which are brittle in nature, are broken up and deformed in the weld region (Fig. 8). The conditions of trial 7 had induced the highest effective stress (2424 MPa) and trial 1 had induced the lowest effective stress (701 MPa) in the rods as shown in Fig. 9.
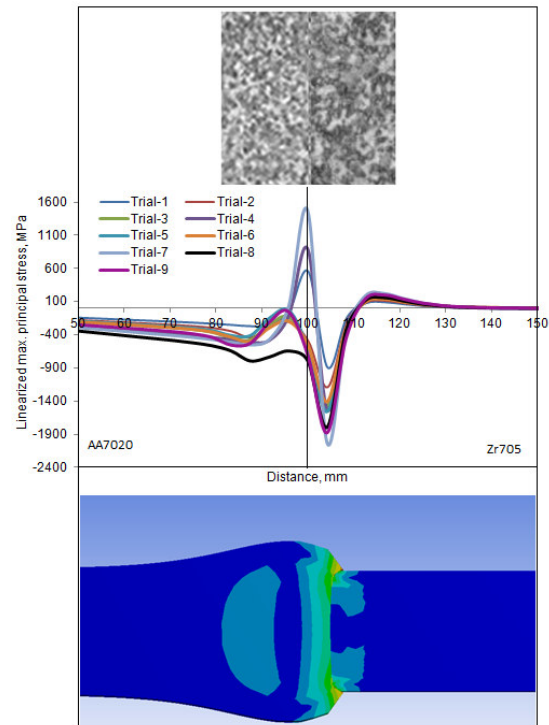

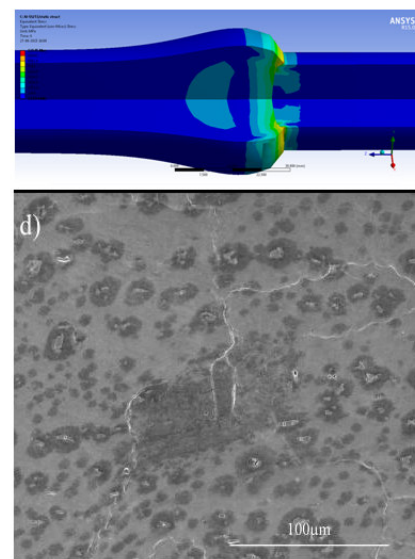Fig. 7. Linearized maximum principle stress induced in weld rods.

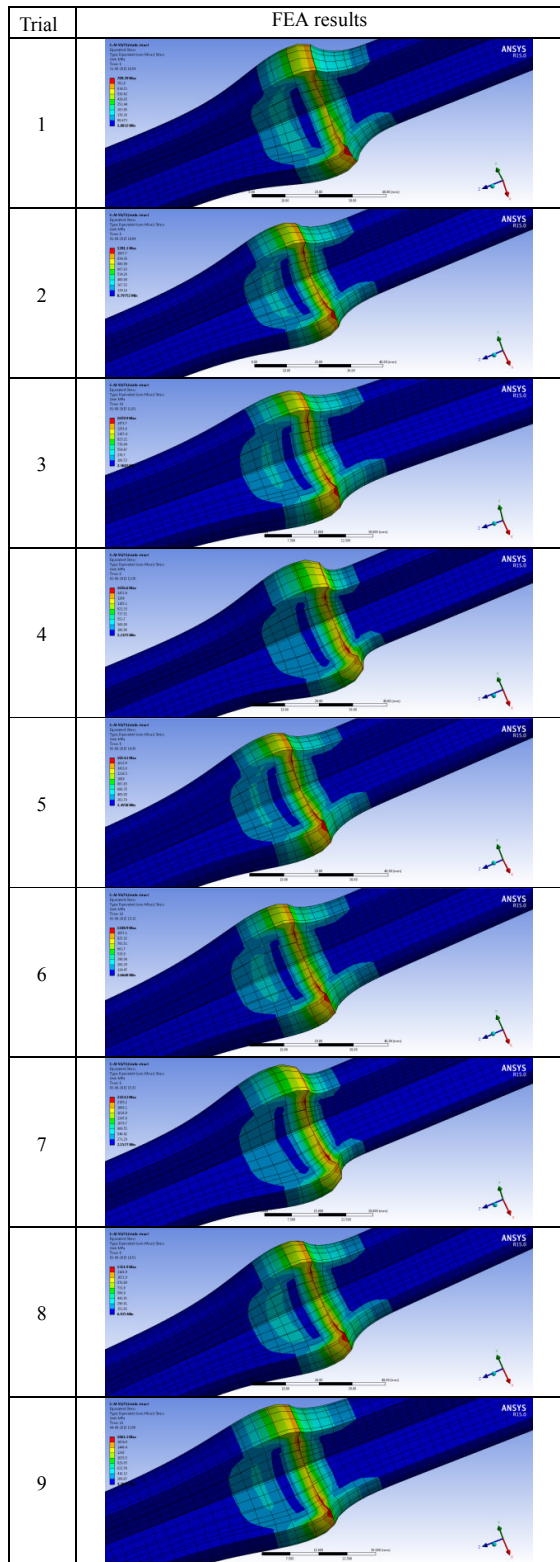Fig. 8. Fracture observed at intermetallic compound.

Trial	FEA results
1	
2	
3	
4	
5	
6	
7	
8	
9	

Fig. 9. Equivalent stress values under different trials.

C. Influence of parameters on bulk deformation

The ANOVA summary of the directional deformation is given in Table 5. The major contributions were of frictional pressure (9.82%) frictional time (32.89%) and rotational speed (40.58%) towards variation in the bulk deformation. The bulk

deformation increased with increase of frictional pressure, friction time and rotating speed as shown in Fig. 10, 11 and 12. In the first numerical iteration the external load would generate uniform pressure on the contact surface and consequently linearly changing heat flux. For the next iteration the pressure distribution on contact surface was calculated Using ANSYS workbench. It was observed that the deformation concentrates mainly near the frictional surface. The extruded shape gradually was formed near the welded joint during the welding process. The extruded shape was asymmetric, as shown in Fig. 14. The tendency of flange formation was higher with AA2024 than with Zr705alloy. This was due to difference in the thermal conductivity and thermal expansion of the two materials. The bulk deformation was found to be maximum (0.58 mm) with conditions of trial 9; whereas it was 0.18 mm with the trial 1 as shown in Fig. 14.

TABLE V.   ANOVA SUMMARY OF THE BULK DEFORMATION

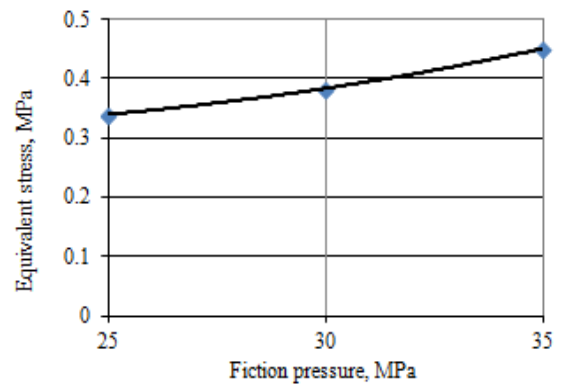| Source	Sum 1	Sum 2	Sum 3	SS	v	V	F	P
A	2.04	2.30	2.70	0.03	2	0.015	6.73	9.82
B	1.79	2.38	2.88	0.09	2	0.045	20.18	32.89
C	1.75	2.35	2.94	0.11	2	0.055	24.67	40.58
D	2.54	0.83	7.04	0.01	2	0.005	2.24	2.13
e				0.02007	9	0.0022297	1.00	14.58
T	8.12	7.86	15.57	0.26007	17			100

Fig. 10. Influence of frictional pressure on deformation
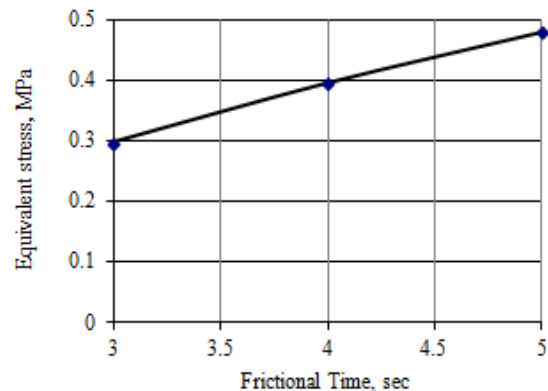
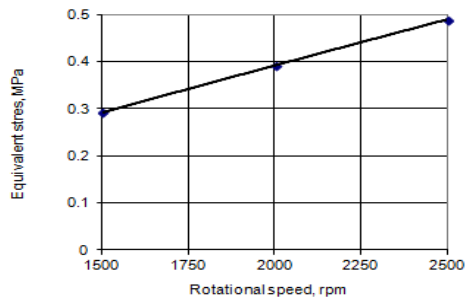Fig. 11. Influence of frictional time on deformation

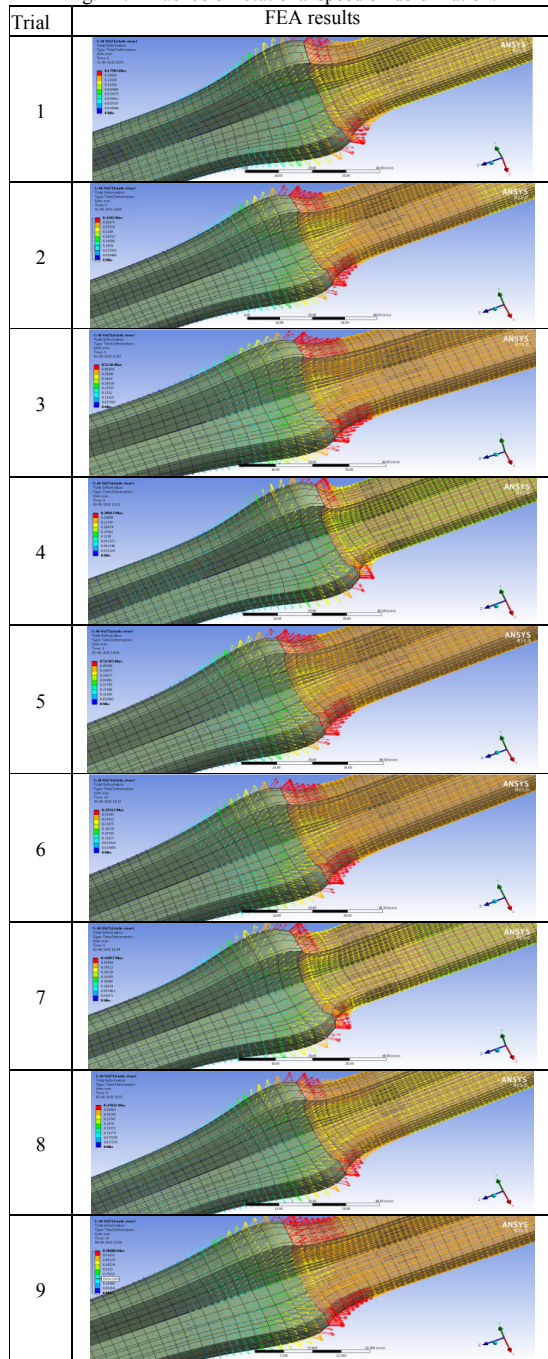Fig. 12. Influence of rotational speed on deformation.

The axial shortening on the AA2024 side was more than that on Zr705 alloy side. Consequently, the material was moved outward forming the flange at the interface. The outward movement of AA2024 was higher than that of Zr705 alloy in proportion to their stiffness characteristics. The elastic module of AA2024 and Zr705 are, respectively, 71.0 GPa and 97.9 GPa. In both the materials the compressive stresses were observed. Thus, the AA2024 material has experienced weld flash at the interface. This is due to the fact that melting point of AA2024 is lower than that of Zr705 alloy.
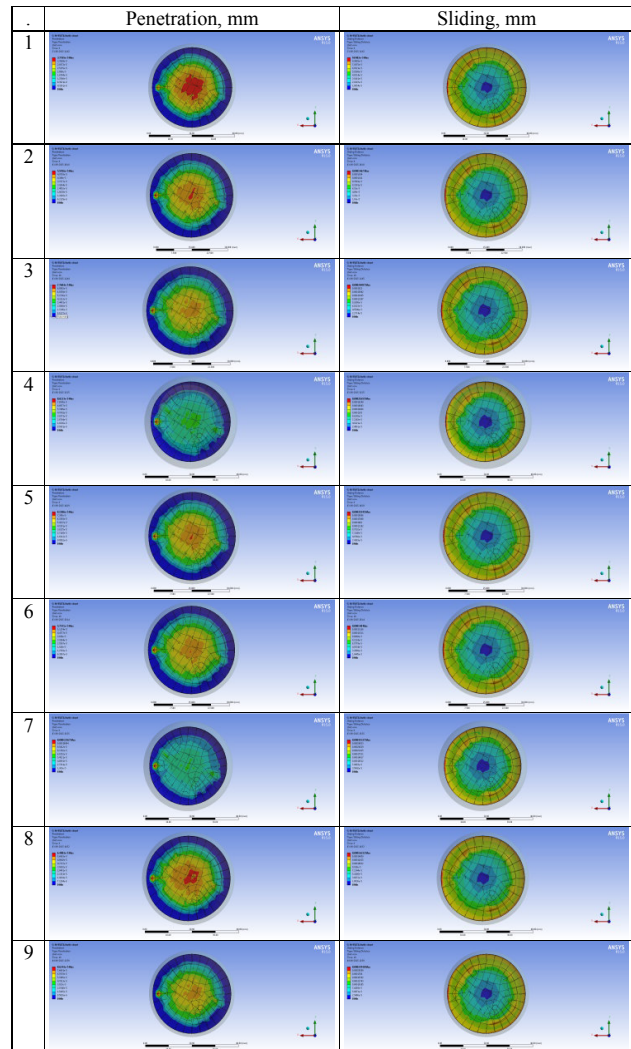
Trial	FEA results
1	
2	
3	
4	
5	
6	
7	
8	
9	

Fig. 14. Bulk deformation values under different trials.

.	Penetration, mm	Sliding, mm
1		
2		
3		
4		
5		
6		
7		
8		
9		

Fig. 15: Penetration and sliding values under different trials.

D. Influence of parameters on penetration and sliding

In friction welding of AA2024-T6 and Zr705alloy, only AA2024-T6 was consumed in the form of flash due to softer material and also due to higher thermal conductivity and coefficient of thermal expansion, as most of the heat generated at the interface was transferred to AA2024-T6. Deformation of Zr705alloy was negligible due to its higher hardness value, and higher melting point as shown in Fig. 16. In the case of trail 1 the interface layer has not produced a good metallic bond between AA2024-T6 and Zr705alloy due to lack of penetration. In the case of trails 3, 5 and 9 the interface layer

has produced a good metallic bond between AA2024-T6 and Zr705alloy on account of deep penetration (Fig. 15).

IV. CONCLUSIONS

This study shows that the AA2024-T6 and Zr705alloy is good if the operating conditions: frictional pressure of 35 MPa, frictional time of 5 sec, rotational speed of 2000 rpm and forging pressure of 31.25 MPa. For friction welding of AA2024-T6 and Zr705alloy, the forging pressure should be 1.25 times the frictional pressure. For this condition of welding there was good penetration and sliding of materials at the welding interface resulting a good mechanical bonding.

REFERENCES

[1] W. Li and F. Wang, "Modeling of continuous drive friction welding of mild steel", Materials Science and Engineering A, (528), pp.5921-5926, 2011.

[2] A. C. Reddy, "Fatigue Life Evaluation of Joint Designs for Friction Welding of Mild Steel and Austenite Stainless Steel," International Journal of Science and Research, ISSN: 2319-7064, Vol. 04, No. 02, pp. 1714-1719, 2015.

[3] A. C. Reddy, Fatigue Life Prediction of Different Joint Designs for Friction Welding of 1050 Mild Steel and 1050 Aluminum, International Journal of Scientific & Engineering Research, ISSN: 2229-5518, Vol. 6, No. 4, pp. 408-412, 2015.

[4] V. Srija and A. C. Reddy, Finite Element Analysis of Friction Welding Process for 2024Al Alloy and UNS C23000 Brass, International Journal of Science and Research, ISSN: 2319-7064, Vol. 4, No. 5, pp. 1685-1690, 2015.

[5] T. Santhosh Kumar and A. C. Reddy, Finite Element Analysis of Friction Welding Process for 2024 Alloy and AISI 1021 Steel, International Journal of Science and Research, ISSN: 2319-7064, Vol. 4, No.5, pp.1679-1684, 2015.

[6] A. Raviteja and A. C. Reddy, Finite Element Analysis of Friction Welding Process for UNS C23000 Brass and AISI 1021 Steel, International Journal of Science and Research, ISSN: 2319-7064, Vol. 4, No. 5, pp. 1691-1696, 2015.

[7] Milton Bernard Hollander, Stamford, William Earl McKinley, Springdale, and Joseph Chin Jung Cheng, Norwalk, Conn., Friction Welding, USS 3,323,203,Patented June 6, 1967.

[8] C.R.Alavala, Finite Element Methods: Basic Concepts and Applications, PHI Learning Pvt. Ltd., New Delhi, 2008.

[9] A. C. Reddy, Finite Element Analysis of Friction Welding Process for AA7020-T6 and Ti-6Al-4V Alloy: Experimental Validation, International Journal of Science and Research, ISSN: 2319-7064, Vol. 4, No. 8, pp. 947-952, 2015.

[10] Sahin M (2010), "Joining of Aluminium and Copper Materials with Friction Welding", pp. 527-534, Trakya University, Edirne, Turkey.